Microsystem Technologies
https://doi.org/10.1007/s00542-024-05673-4

TECHNICAL PAPER

Hybrid cable tension–length compensation algorithm for dynamic performance improvement of mobile cable-driven parallel robot

Dong-Yeop Shin[1] · Byeong-Geon Kim[1] · Jin-Hwan Lim[1] · Seok-Gyu Hong[1] · Kyoung-Su Park[1]

Received: 30 December 2023 / Accepted: 4 April 2024

Abstract
This paper investigates a new approach for the control of Mobile Cable-Driven Parallel Robots (MCDPR) called the Hybrid tension–length compensation algorithm (HTLCA). The Cable-Driven Parallel Robot (CDPR) system controls the end-effector using cables, which is a different system structure from robots with rigid arms or Cartesian methods. The MCDPR combines with a mobile robot to overcome the limitations of the CDPR system, such as limited spatial mobility and the ability to achieve a larger workspace, providing higher degrees of freedom and efficient working space. However, there is currently no robust solution to control the end-effector in real-time and stability in dynamic environments. Therefore, this study proposes the HTLCA to compensate for control errors caused by various factors in dynamic environments. The proposed algorithm performs hybrid force and length closed-loop PID control using the calculated tension distribution algorithm (TDA) values of the cables for the end-effector position, target length values, and the measured tension distribution and length values of the current cables. Experimental results using the proposed HTLCA algorithm in CDPR and MCDPR modes show a 57.20% reduction in tension control errors compared to before its application in a mobile robot's driving environment. Therefore, HTLCA effectively compensates for errors by simultaneously controlling the tension distribution and length of the cables, improving dynamic performance, and ensuring stable control, thus demonstrating its validity.

1 Introduction

The Cable-Driven Parallel Robots (CDPRs) are have unique advantages such as high end-effector weight and payload ratio (Bostelman et al. 1993), with lightweight and low inertia effector, can drive high-speed operation based on wires (Zhang et al. 2018; Morizono et al. 1998; Kawamura et al. 2000), and a wide range of workspace spectrum from small (Morizono et al. 1998) to large-scale operations (Yao et al. 2013; Brown 1985; Wang et al. 2014). These robots are utilized in various fields such as simulation of low-gravity environments (Wang et al. 2014), sky-camera (Brown 1985) wind tunnel experiments (Lafourcade et al. 2002), construction sites (Bostelman et al. 1993), underwater operations (Bostelman and Albus 1993), planetary exploration (Bostelman et al. 1994), radio telescopes (Yao et al. 2013), virtual environment training (Morizono et al. 1998) and high-speed pick-and-place tasks (Zhang et al. 2018), and rehabilitation exercises (Rosati et al. 2005; Mao et al. 2014). However, due to the unmodeled system elements, nonlinear characteristics of cables, and uncertainties in the system model (Babaghasabha et al. 2015; Ji et al. 2020), stable control of CDPRs is challenging, and their dynamic performance is often degraded.

In recent years, several studies have been conducted to improve the dynamic performance of CDPRs. Since the size of the workspace is influenced not only by the geometric length of the cables but also by the actual distribution of forces in the controlled cables, it is necessary to calculate the ideal cable tension distribution within a feasible workspace (Tho and Thinh 2022; Gosselin 2014) and keep it within a predetermined tension range with Tension Distribution Algorithm (TDA) (Carpio-Alemán et al. 2018; Côté et al. 2016; Fabritius et al. 2023; Gouttefarde et al. 2015; Tho and Thinh 2022) to prevent malfunctions of the robot. To control an end effector with n degrees of freedom, at least n + 1 wires are required (Kawamura et al. 2000). Additionally, to ensure stable control, 2 additional

✉ Kyoung-Su Park
pks6348@gachon.ac.kr

[1] Department of Mechanical Engineering, Gachon University, Seongnam-si, South Korea

Published online: 24 April 2024

degrees of freedom are used (Gouttefarde et al. 2015; Lafourcade et al. 2002; Yao et al. 2013). A 2-redundancy degree of freedom system was evaluated to achieve stable control by various methods, such as separating the force and length control sets and controlling the cable with minimum tension (Mattioni et al. 2022), resolving the CDPR's redundant 2-DoF control problem. A real-time path planning algorithm for CDPRs in dynamic environments based on an artificial potential guide RRT has been proposed for dynamic stability (Xu and Park 2020, 2022; Xu et al. 2023a, b). And various controllers considering uncertainties and exceptions in different systems have been designed, such as an adaptive robust sliding mode controller considering unmodeled system model uncertainties (Babaghasabha et al. 2015), an adaptive synchronization control considering synchronization errors (Ji et al. 2020), a calculation processing of tension distribution outside the workspace (Gouttefarde et al. 2015), and force compensation applied when exceeding the tension limit of a CDPR (Fabritius et al. 2021). Despite these advancements, effectively compensating for the cable tension–length dynamics in CDPR remains a challenge.

To achieve a more flexible workspace and adaptable working environment, recent developments in CDPR systems have introduced reconfigurable parallel robot designs (Gagliardini et al. 2018; Oh et al. 2006) that allow for the adjustment of the size and position of the workspace by adjusting the position of the Pulley-Winch on the Frame. However, these systems still only allow for reconfiguration along limited fixed axes. Therefore, research is currently underway to develop Mobile Cable-Driven Parallel Robot (MCDPR) systems that combine each Z-axis of the Frame with a mobile robot base, enabling further reconfiguration possibilities.

The MCDPR system introduces mobility to the CDPR system, allowing for portable and expandable workspace (Pedemonte et al. 2020; Tan et al. 2020), and enhancing its diversity. To control this MCDPR system effectively, more sophisticated control strategies are required for cable and path generation. Research in this area includes system modeling (Pedemonte et al. 2020), mechanical stability based on it (Tan et al. 2020), calculating stable tension through cable tension distribution, and evaluating tension stability considering tipping condition using MZP conditions (Pedemonte et al. 2020; Rasheed et al. 2018; Xu et al. 2023a, b). Furthermore, the motion equations of the MCDPR system are presented, and a controller based on input–output linearization is proposed (Korayem et al. 2017). Additionally, path planning for the end effector and mobile base considering the Feasible Tension Set and Workspace is crucial, and various methods such as direct transcription (Rasheed et al. 2019) and real-time path planning based on the RRT algorithm have been studied for path planning in a 4-mobile base, 4-cable, 3-DOF MCDPR system (Xu et al. 2023a, b).

However, despite the efforts of previous research on MCDPR, the consideration of the equilibrium of the mechanism based on stable control conditions and the kinematics have been well theoretically modeled (Korayem et al. 2017; Pedemonte et al. 2020; Rasheed et al. 2018, 2019; Tan et al. 2020; Xu et al. 2023a, b). However, they did not consider the complexity caused by the additional degrees of freedom due to the added mobile robot base, the precision problem of localization of distributed nodes that frequently occurs in the control of mobile robots, and various environmental factors such as control delay and errors caused by the actual dynamic characteristics. Furthermore, these values are reflected in the fixed variables of the uncertainty model mentioned in previous research, rendering the proposed methods for cable length and kinematic calibration and stability determination meaningless. This is a limitation that arises.

To address these issue, various correction methods for Kinematics in the CDPR system have been proposed (Jeong et al. 1998; Nguyen and Caverly 2021). However, implementing them in real-time in the MCDPR system would significantly increase computational costs and pose difficulties due to the lack of calculation freedom. Therefore, the dynamic performance of real-time control models and controllers in such incomplete systems still suffers from significant control errors, as effective compensation for cable tension–length dynamics is lacking.

Furthermore, while there have been studies simulating fully constrained systems using 8 cables for 4 mobile robots (Xu et al. 2023a, b), there is a lack of systems that have performed control and analysis. Some studies have limited the motion of the end effector by using 8 cables for 2 robots (Pedemonte et al. 2020) or 4 cables (Rasheed et al. 2018), while others have conducted limited experiments using a system consisting of 3 mobile bases with restricted degrees of freedom and a telescopic rod (Tan et al. 2020).

as mentioned above, various research has been conducted to include uncertainty models for stable control of MCDPR, but the non-modeled environmental factors such as cable and system nonlinearity, localization errors of distributed nodes, slipping, and command synchronization errors due to communication delays distort the Kinematics of the system, significantly affecting performance. Previous studies have not addressed these issues or how actual cable control is performed, and there has been no research conducted on experimentally controlling an 8-cable MCDPR system with a 6-DOF End-Effector stably.

Therefore, this study aimed to develop a cable controller to compensate for the dynamic instability of cable control caused by Kinematics distortion due to various environmental factors in reality. To achieve this, a hybrid tension–

length compensation algorithm (HTLCA) was developed to control force and length simultaneously. This algorithm allows each mobile robot to control the cable length based on Online Kinematics independently without relying on a central controller, while effectively compensating for Kinematics distortion caused by unmodeled uncertainty variables by controlling the cable tension based on stable tension distribution from TDA.

Ultimately, this approach effectively addresses system model uncertainties such as cable and system nonlinearity, and control delays, enhancing the dynamic performance and robust control of MCDPR significantly.

This paper performs the modeling of the system through the calculation of Inverse Kinematics based on the positions of each joint of MCDPR and the coordinates of the end effector, which are necessary to construct HTLCA. This is done in Sect. 2.1. Using this kinematics, the lengths of the 8 cables (8DoF) that control the position and pose (6DoF) of the end effector are calculated by utilizing the position information of the end effector and the mobile robot. In this calculation, the two extra degrees of freedom are used to estimate the stable tension distribution at the target point, which is defined as the TDA in Sect. 2.2. The communication structure of the experimental setup for applying this is defined in Sect. 2.3. Then, HTLCA is designed by merging TDA with the controller of MCDPR Cable and communicating with it. This is described in Sect. 2.3. Next, the experimental setup to validate proposed HTLCA is presented in Sect. 3.1. The experiments to be conducted in this experimental setup are defined in Sect. 3.2, and through these experiments, it is verified whether HTLCA improves the dynamic performance of the MCDPR system.

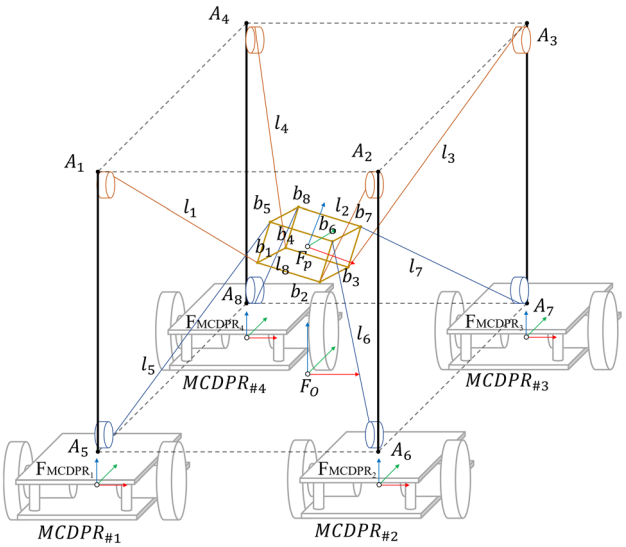

Fig. 1 MCDPR system model

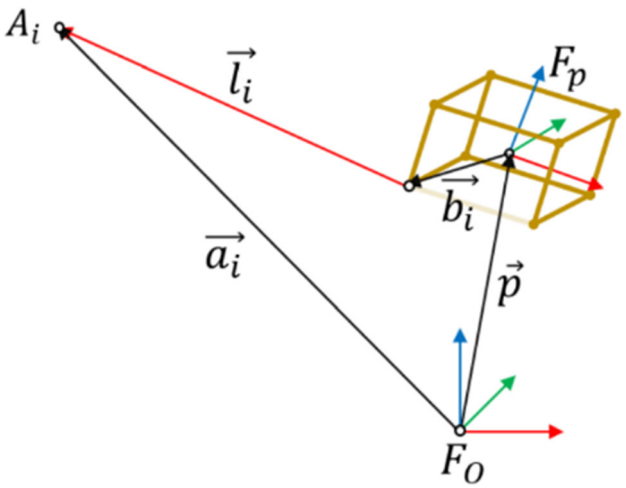

Fig. 2 End-effector and anchor point vector loop

2 Theoretical Background

2.1 MCDPR system modeling and notation

This chapter, we perform modeling for the control of the MCDPR system. The model of the MCDPR used in the experiment is structured as shown in Fig. 1.

The vector relationships of each cable $i \in 1, \ldots, m$ can be expressed as follows. A_i represents the Anchor Point where the n-th cable comes out in the F_O frame. Additionally, B_i represents the point where the n-th cable is connected to the end effector in the F_p frame. Furthermore, l_i represents the length of the cable from Anchor Point A_i to B_i. The vector relationships for the Anchor Point, end effector exit, and frame origin are shown in Fig. 2.

This relationship can be expressed as the vector Eq. (1) for the cable vector $\vec{l} = [l_1 \ldots l_m] \in R^m$, and each of the m cable numbers is denoted as $i \in 1, \ldots, m$.

$$\vec{l}_i = \vec{a_i} - \vec{p} - R_P \vec{b_i} \tag{1}$$

In this case, the Global-zero = fixed coordinate system = origin coordinate system is denoted as $\mathcal{F}_\mathcal{O}$. The coordinate system of the end-effector (EE), which performs the control, is represented as $\mathcal{F}$, and the vector pointing towards the end-effector connection point B_i of each cable from the center of the F_p frame is defined as $b_i \in R^3$. The DoF of CDPR is constrained by the pose consisting of the position and rotation elements of the platform, where the position $\boldsymbol{p} \in \mathbb{R}^3$ represents the coordinate displacement in 3-dimensional space with elements of x, y, z coordinates.

Furthermore, the Rotation $\boldsymbol{R_P} \in \boldsymbol{SO}_3$ represents the coordinate system rotated by the Kardan Angle ϕ of the EE, and can be written as Eq. (2) in the same way.

$$R_P = R_x(\phi_{O,x})R_y(\phi_{O,y})R_z(\phi_{O,z}) \tag{2}$$

The length of the cable required for control, l is show in Eq. (3), and the direction vector of the cable, $\overrightarrow{u_i}$, can be determined as shown in Eq. (4).

$$l_i = \left|\left|\overrightarrow{l_i}\right|\right| \tag{3}$$

$$\overrightarrow{u_i} = \frac{\overrightarrow{l_i}}{||l_i||} \tag{4}$$

2.2 Tension distribution calculation algorithm (TDA)

We construct the Structure Matrix $A^T \in R^{n\times m}$ for MCDPR using the cable direction vector u_i, which is represented by Eq. (4), and the rotation matrix R_P for the Pose frame of the EE. We also use the vector b_i, which represents the distance from the center of the EE Frame $\mathcal{F}$ to the cable attachment anchor point.

$$\mathbf{A}_i^T = \begin{bmatrix} u_i \\ R_P b_i \times u_i \end{bmatrix} \in \mathbb{R}^6 \tag{5}$$

Furthermore, the force F and the moment M of the wrench w can be expressed as Eq. (6), considering the external forces and the force of gravity.

$$w = \begin{bmatrix} F_x \\ F_y \\ F_z \\ M_x \\ M_y \\ M_z \end{bmatrix} \tag{6}$$

In conclusion, the system has a degree of freedom of n = 6 DOF, which is parameterized by the position vector $\boldsymbol{b} \in \mathbb{R}^3$ and the rotation matrix $\boldsymbol{R_P} \in \boldsymbol{SO}_3$. By using the structure matrix obtained above and the load on the end effector, the tension vectors of the cables, which are the forces acting on each line, can be simply calculated. These tensions must be physically greater than 0, smaller than the maximum allowable tension T_{max} that the mechanism can handle and satisfy T_{min} to prevent cable sagging and maintain the normal position. The tensions $\boldsymbol{f}$ that satisfies these conditions can be calculated as shown in Eq. (7).

$$\mathbf{A}^T f = -w \text{ subject to } 0 \le T_{min} \le f \le T_{max} \tag{7}$$

If the above tension limit is satisfied, it can be considered as a feasible cable tension. However, in this case, a negative tension can be calculated for the cable located below. Since cables cannot transmit negative tension, this results in a physically impossible, this means non-feasible solution. To solve this issue, an additional homogeneous solution f_{int} in the null-space of the structure matrix is added using the inhomogeneous solution f_{ext} from the equilibrium Eq. (7) due to external forces and the surplus degrees of freedom caused by constraints. This adjustment allows for a feasible solution in the control domain. The general solution to this problem is expressed as Eq. (8) as introduced by Kraus (2016)

$$f = \underbrace{-\mathbf{A}^{+\mathrm{T}}\mathbf{w}}_{\mathrm{f_{ext}}} + \underbrace{\mathrm{H}\lambda_{\mathrm{H}}}_{\mathrm{f_{int}}} \tag{8}$$

At this point, A^{+T} is the Moore–Penrose pseudo-inverse of the Structure Matrix A, and H is the Null-Space of the Structure Matrix A. Various algorithms exist for finding the Homogeneous Solution noted at (Kraus 2016), but in this study, the central value of the given maximum/minimum tension control condition,f_{ref}, is used, and it can be written as Eq. (9).

$$f_{ref} = \frac{T_{max} + T_{min}}{2} \tag{9}$$

Through this, we can obtain the optimal f_{cf} that minimizes the Euclidean norm between the tension $\boldsymbol{f}$ and the reference tension f_{ref} specified in Eq. (9) through second-order norm optimization, as shown in Eq. (10).

$$f_{CF} = f_{ref} - A^{+T}\left(w + A^{+T} f_{ref}\right) \tag{10}$$

Equation (10) can be rewritten as the following Eq. (11) in a simplified manner.

$$f_{CF} = -A^{+T} w + \left(I - A^{+T}A^T\right) f_{ref} \tag{11}$$

The TDA is a series of calculations based on the kinematics of the MCDPR system, which allows for the calculation of tension distribution between the mass and tension control targets of the Geometry and End Effectors. This algorithm enables the determination of the tension distribution in the system.

2.3 Communication structure between master and mobile nodes

The MCDPR system is a communication system for controlling actual cables, as shown in Fig. 3. The system consists of a Master Controller, Mobile Node Controller, HTLCA Controller, and Cable Controller hardware, which communicate with each other through ROS2.

The Master Controller calculates the TDA and cable length and transmits them, while receiving real-time Kinematics information from each Mobile Node Controller. This synchronous communication between distributed nodes is implemented using ROS Actions.

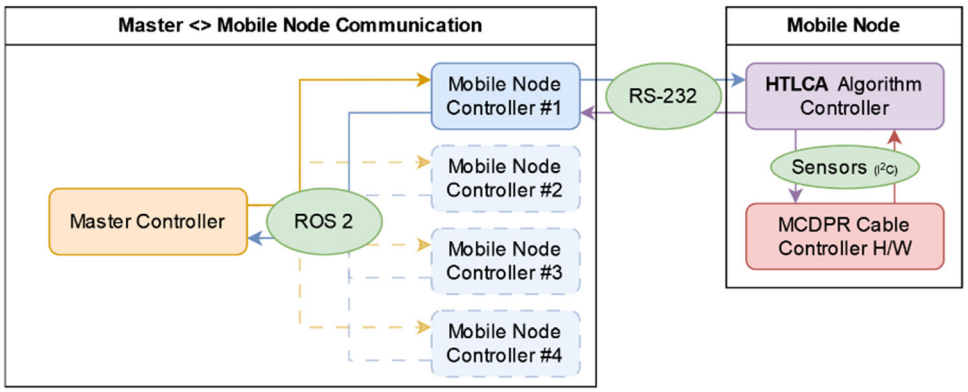

Fig. 3 Mobile, master communication structure with ROS2

The Mobile Node Controller receives the TDA and length from the Master Controller and processes them through an Extended Kalman Filter, along with IMU data and other information. Additionally, it reports information such as the movement and odometry of the Mobile Robot, real-time cable length, and tension values to the Master Controller.

The HTLCA controller directly controls the motors of the Mobile Node hardware and constructs a closed loop circuit using the current tension and cable length from the sensors. It performs hybrid PID control of the target tension/length using this information. As a result, each node operates independently, eliminating synchronization overhead and control time delays with the Master.

2.4 Definition and structure of HTLCA

Normally, the cable controller operates by moving the end effector towards the target point P_{target} from the current point P_{now} while also moving the mobile robot as shown in Fig. 4. However, in real mobile robot environments, it is difficult for all the robots to ideal kinematics and flawless communication with the master node while driving dynamic conditions. Therefore, simply controlling the cable length is not sufficient to compensate for these errors in a stably. To address this, we devised an HTLCA controller that simultaneously performs tension and length control. A detailed operation of the HTLCA controller to correct the length control through force control inside Fig. 4 could be rewritten by following Eq. (13).

$$PID_i(e_i, \mathrm{dt}) = \begin{bmatrix} K_p & K_i & K_d \end{bmatrix} \begin{bmatrix} e_i \\ \sum_0^i e_i \\ \dfrac{e_i - e_{i-1}}{\mathrm{dt}} \end{bmatrix} \tag{12}$$

$\mathrm{PID_i}$ is defined as the classical i-th incremental PID controller with $\mathrm{K_{p,i,d}}$ gains as the proportional coefficients of the proportional/integral/derivative terms of each error input (e_i) and execution time (dt) as Eq. (12).

$$\underbrace{\begin{bmatrix} L_{T_{abs}} \\ t_T \end{bmatrix}}_{\substack{absolute \\ controloutput}} = \sum_{i=0}^{\frac{t_C}{dt}} \underbrace{\begin{bmatrix} PID_i(T_{TDA} - T_{now}, \mathrm{dt}) \\ \mathrm{dt} \end{bmatrix}}_{\substack{incrementalrelative \\ control0.25emoutput}} + \begin{bmatrix} L_C \\ 0 \end{bmatrix} \tag{13}$$

First, from Fig. 4 the Master node performs calculation and transmission of the stable target tension TDA (T_{TDA}) using Eq. (11), the control time (t_C), and the absolute target position of the cable (L_C) for the mobile robots. once receiving these values, the HTLCA (work as lower-level cable controller) start working and stores them in variables. The Dynamixel controller for cable control receives the final absolute position ($L_{T_{abs}}$) and control target time (t_T) as input. As the received control target time and cable position decrease over iterations, the remaining ratio of the control target time for this iteration is calculated by accumulating the time taken in past iterations and subtracting it from the absolute control time received from the master node, and then dividing by the time taken for the iteration (dt) to calculate the time scale for adjusting the control values over time. note that the relative to absolute cable position conversion is simplified in Eq. (13). Therefore, the absolute target position for this iteration is calculated as the sum of the PID_i value due to the error between the ideal tension(T_{TDA}) and the currently measured tension(T_{now}), multiplied by the time-scale for the scale by remaining target time, and the sum of absolute target position of the cable (L_C).

Thus, when performing PID control as in Eq. (13), the PID_i term due to tension control length error converges to 0, and the control time is precisely reached($L_{T_{abs}} \approx L_C$) by performing iterations$(0, 1, \ldots, \mathrm{i})$ until the reach to target time($\mathrm{t_c}/\mathrm{dt} = \mathrm{i}$). at control end, as shown in Fig. 4, the mobile node notifies the higher-level controller that the cable length control has been completed. Even if there are errors or delays in the commands from the higher-level controller, or if the mobile robot slips or localization is off, the HTLCA controller will still perform PID control on the

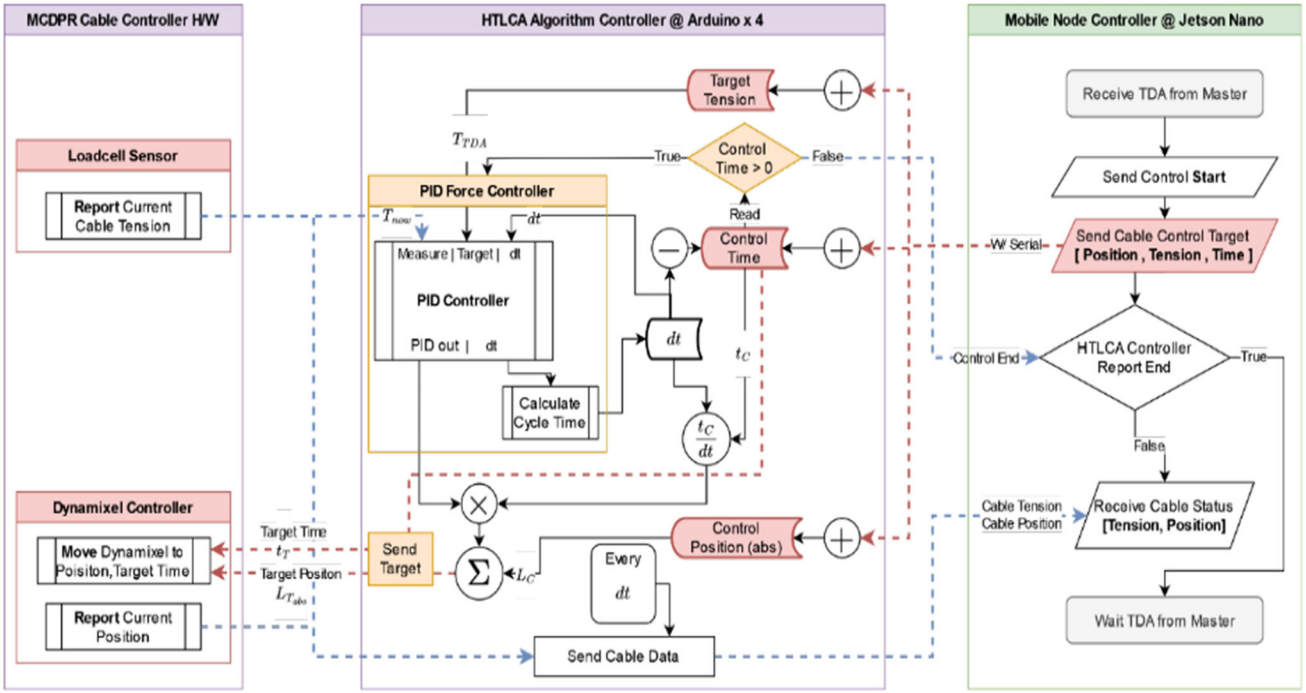

Fig. 4 Structure of HTLCA method

tension distribution of the target to maintain control of the end effector as much as possible.

3 Experimental design and results

3.1 Stationary/moving MCDPR experimental hardware and setup

We implemented the MCDPR setup described above for conducting experiments, using the ROS2 framework for control and communication. The entire MCDPR system consists of a Master (PC) Node that performs waypoint and path calculations and issues commands, and a Drive Node that handles actual driving and cable control. The MCDPR hardware includes traditional CDPR control components such as an End-Effector for manipulating the payload, a Dyneema Cable for force transmission, Dynamixel Motors for cable actuation, and a Winch System. These components are combined with a mobile base to form the MCDPR system, and a load cell was used for tension monitoring during experiments. The closed-loop control and data logging of the Dynamixel Motors and load cell are performed by a lower-level Arduino controller, including an HTLCA controller. The synchronization between the mobile robot and the master PC is performed by the Mobile Controller Node, which is a Jetson Nano, as mentioned in Sect. 2.3. The Drive Node, using ROS2, receives target position information from the Master PC and controls the wheels to move to the target location.

The target cable tension calculated by the TDA algorithm in the Master Node is propagated to each mobile node and assigned to it. The mobile nodes that receive this assignment transmit the control values to the Arduino, which then uses the HTLCA controller to follow the target cable tension and length. The load cell data is used to measure the stability and precision of the control, and the experimental results are analyzed accordingly.

3.2 Experiment design of MCDPR in stationary and moving states

Stationary MCDPR control experiment is unlike as traditional CDPRs, MCDPRs may stop to perform tasks such as construction after driving, and in situations where localization errors and slips occur. Furthermore, because MCDPRs do not have a rigid frame like CDPRs, they are subject to tensions as low as the cable on flat ground, or even less if the task is performed on an inclined position, which can cause the mobile robot to be lifted by the tension and dislocate or fall (Pedemonte et al. 2020; Rasheed et al. 2018; Xu et al. 2023a, b). Through multiple experiments, we observed an average localization error of 5 mm due to placement and wheel backlash. Thus, the experiment is conducted in an environment with a placement error (avg. $\sim$ 5 mm). it is verified whether the system cable load caused by misaligned time-invariant kinematics

uncertainty can be effectively reduced. The detailed description of this experiment is as follows.

The end effector path of the Stationary MCDPR is shown in Fig. 5. The mobile robot is designed to remain stationary. For the Stationary MCDPR experiment, we conducted experiments for both cases with and without HTLCA. The actual experiment was conducted in an environment in Fig. 6.

Moving MCDPR experiment is MCDPR in an environment with real-time localization error (average of approximately 50 mm). Through multiple experiments, we observed an average localization error of $\sim$ 50 mm due to slipping on the surface and integration error of the IMU. This led us to perform these experiments. The driving paths for MCDPR#1 $\sim$ 4 and the end effector are shown in Fig. 7a. The experiments were conducted in two conditions based on the presence or absence of the HTLCA in the MCDPR, and the actual experimental environment is depicted in Fig. 7b.

3.3 Experimental results and analysis

Graphs of each stationary MCDPR experiment result, the units are all [gf], and RGBK colors are assigned to MCDPR #1–4. Figures 8 and 9 show the graphs where the target TDA, which should be theoretically followed, is represented by dashed lines, and the controlled and measured tension values are represented by solid lines. The tension data was measured in the experiments conducted to validate the effectiveness of HTLCA in controlling the end effector in Stationary MCDPR control experiments with a consistent initial error during placement. The results of the experiments, both with and without using HTLCA, are as follows.

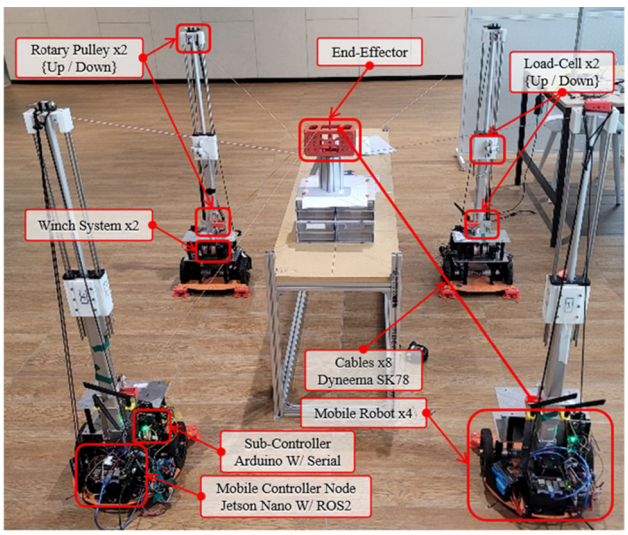

Fig. 5 Stationary MCDPR experiment path

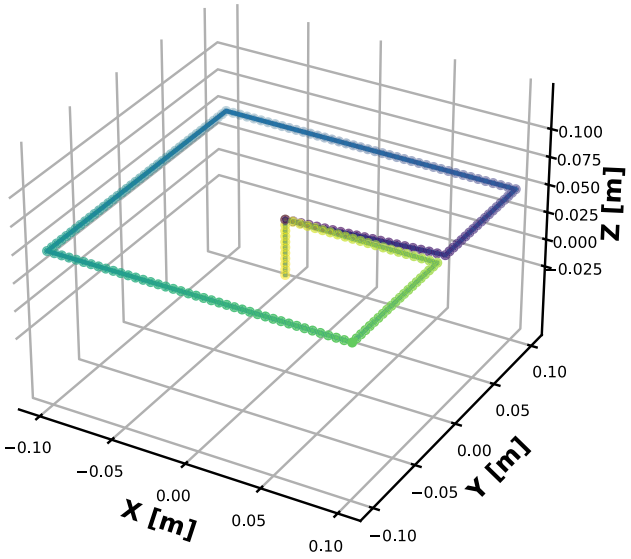

Fig. 6 MCDPR setup for experiment

In the stationary MCDPR experiment, when HTLCA was used, the maximum tension was measured as 275 gf. On the other hand, in the experiment without using HTLCA, the maximum tension was measured as 613 gf. When HTLCA was used, the tension distribution showed a consistent movement around the target tension value, exhibiting a regular pattern. However, in the case without using HTLCA, it was observed that there were continuous large peak tensions at specific positions.

Next, in the Moving MCDPR control experiment where the end effector is controlled simultaneously with driving in a dynamic state where errors in Geometry, Localization, IMU integration, etc. accumulate, the data on tension caused by the use or non-use of HTLCA was measured.

In the MCDPR experiment, when using HTLCA, the maximum tension measured was 249 gf, whereas without using HTLCA, the maximum tension measured was 512 gf. Furthermore, when using HTLCA, a similar trend was observed for the target tension values and measured tension values, showing regular movements. However, when HTLCA was not used, the calculations did not match the actual values, resulting in excessive tension at certain positions, causing the control to fail after the peak tension. This led to the cable getting tangled and hanging in mid-air, with the lower cables being uncontrolled and experiencing tension levels around 0 gf.

3.4 Experiment data analysis

In the MCDPR experiment, the difference between the real-time calculated target tension and the measured tension was used as the analysis data. This was done to interpret the behavior in the tension dimension by

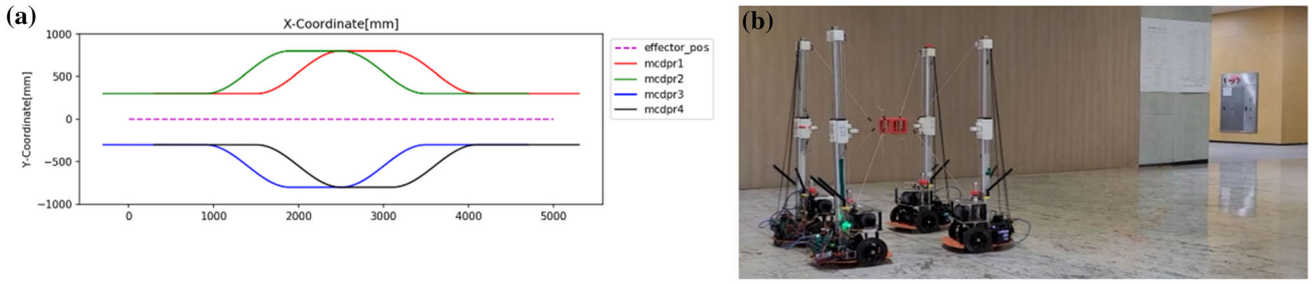

Fig. 7 **a** Moving MCDPR experiment path. **b** MCDPR control experiment environment

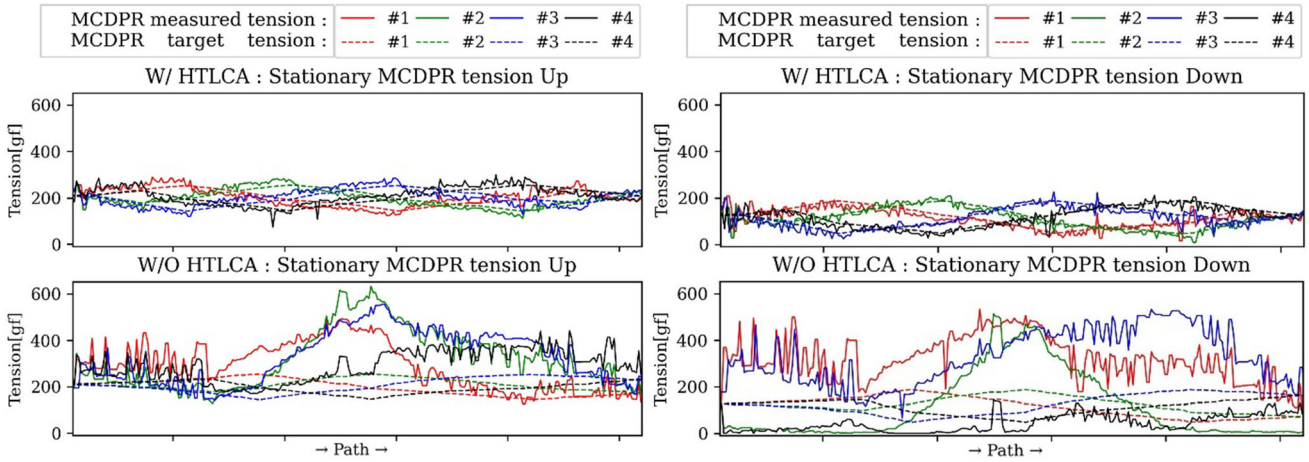

Fig. 8 Stationary MCDPR exp. tension—up, down

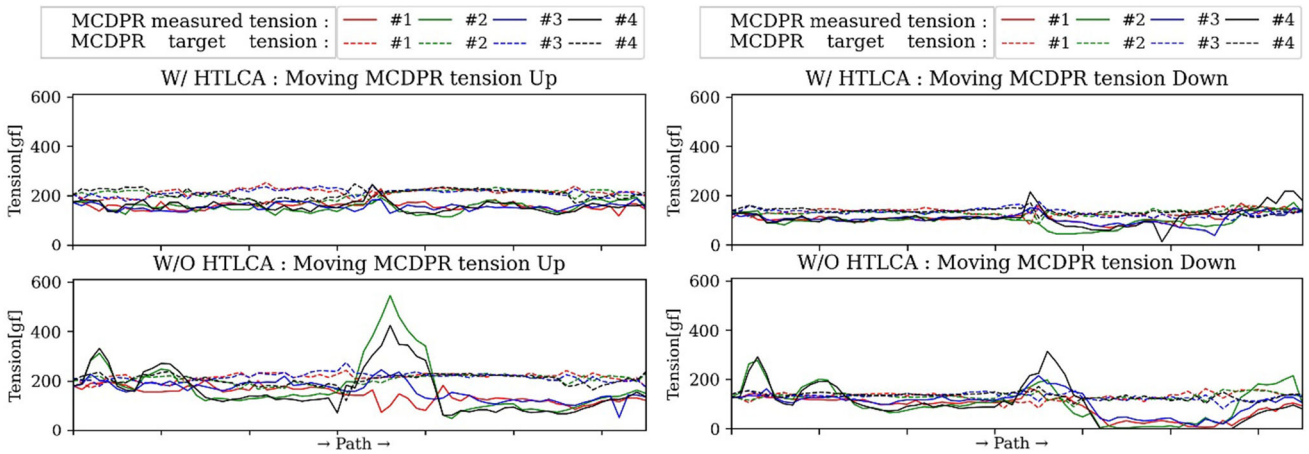

Fig. 9 Moving MCDPR exp. tension—up, down

graphically representing the arithmetic error between the stable tension value and the actual control value of the experimental data.

Additionally, Kernel Density Estimation (KDE) analysis was employed to quantitatively evaluate and compare the actual control values for each cable's TDA input. This involved estimating and analyzing probability density functions for the two different experiments using KDE. The data distribution was visualized and compared based on this analysis and quantitative evaluation performed.

In the MCDPR experiment, the coordinates of the MCDPR mobile base are fixed, and the tension control error graph Fig. 10 and KDE analysis data for the stationary MCDPR experiment, which models setup errors, localization, and communication delays of the MCDPR system, are shown in Fig. 11.

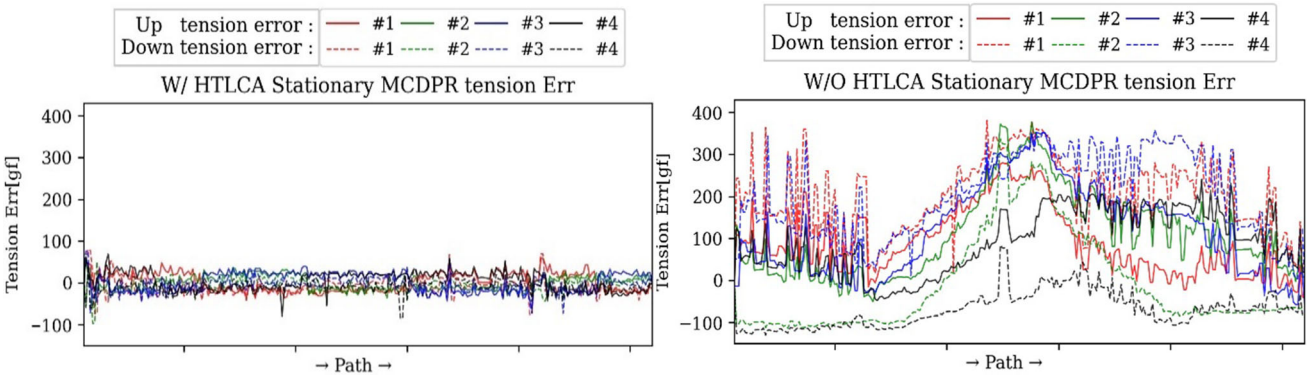

Fig. 10 Stationary MCDPR T_{err}—W/, W/O HTLCA

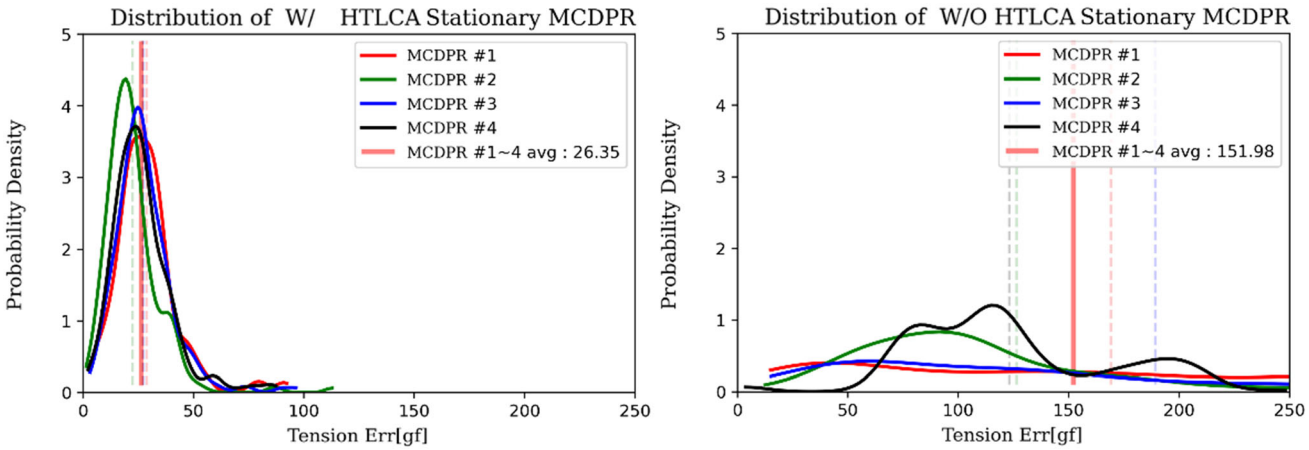

Fig. 11 Stationary MCDPR KDE PDF function W/, W/O HTLCA

Figure 10 shows the arithmetic error between the controlled tension value Eq. (11) and the actual controlled value for the Stationary MCDPR experimental data, with and without the HTLCA algorithm. When the HTLCA algorithm is not applied, the tension control error value diverges and increases noticeably. This indicates that there is a critical effect on error in the kinematics due to small initial setup errors and jittering communication delay, etc., which is not corrected and requires compensation in the control. On the other hand, when the HTLCA algorithm is applied, there is no divergence or significant increase in tension observed. Instead, it converges to a stable range of tension control and demonstrates effective control.

next, presents the KDE graphs for each experiment, providing a quantitative evaluation. The average tension control error and the maximum value of the probability density function (PDF) are analyzed using KDE.

the quantitative evaluation of each experiment can be seen in the KDE graphs in Fig. 11. The average tension control error and the maximum value of the PDF are evaluated. Using the HTLCA, the average tension control error decreases from 151.98 gf to 26.35 g, and the maximum value of the KDE PDF increases to 1.13 and 4.34. This effectively stabilizes the tension distribution to follow the ideal tension distribution. Additionally, the maximum measured tension decreases from 613 to 275 gf, confirming that the actual tension control operates effectively without divergence.

The following is tension error analysis of Moving MCDPR Experiment measurement data in terms of tension dimension resulting from the use of HTLCA in Moving Control, where geometry, localization, and IMU integration errors which not constant, accumulating error in a dynamic state during driving experiments.

In this Moving MCDPR experiment, it was observed that when HTLCA was not used, the calculations did not align with the actual values, as indicated in Fig. 12, due to the presence of several errors mentioned earlier. In such an environment, the main points of the Tension error measurement are as follows. This maximum tension tends to occur when the MCDPR nodes are scattered and gathered on the driving path shown in Fig. 7a, and it appears to be mainly localization data influenced by the ground slippage and nonlinearity of the wheels due to curved driving. As a

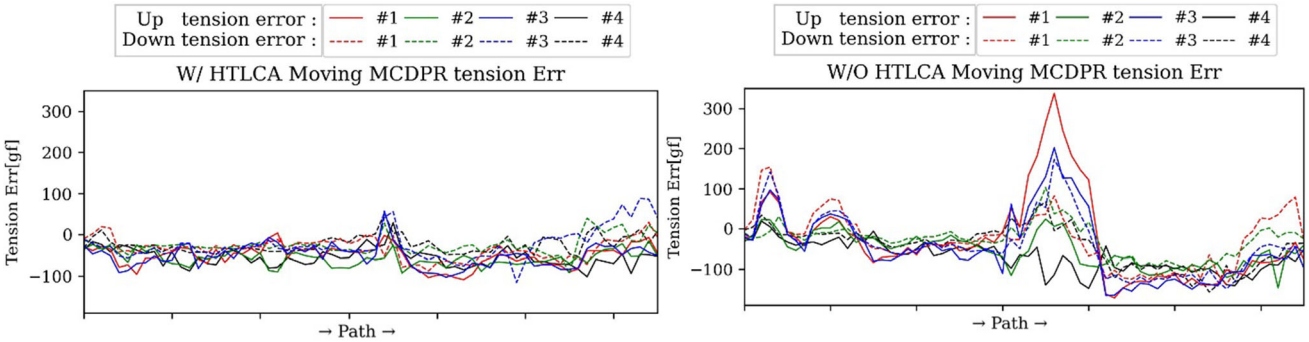

Fig. 12 Moving MCDPR T_{err}—W/, W/O HTLCA

result, at certain positions, the tension became significantly higher than the control target value, and after reaching the peak tension, the control of the end effector failed, causing the cable to become entangled and hang in mid-air. As a result, the tension in the lower cable was observed to be at a level of min ∼ 0 gf, indicating that it was not under control. However, when using HTLCA, a tendency was observed to follow the target tension value during the scattering and muster runs, and it was confirmed that it successfully compensated for the previously identified nonlinearity and localization errors.

At this point, the KDE PDF function data of MCDPR Moving Expr. for quantitative evaluation data is like the fixed MCDPR Exp. in Fig. 11. When HTLCA is applied, the tension error at the highest probability density points and the mode position decreases from 95.99 gf to 65.33 gf, and the maximum value of the probability density function increases from 0.98 to 1.75. This confirms that the HTLCA algorithm effectively follows the ideal tension, even in intense nonlinear elements such as delays or gathering during operation. Additionally, the maximum system tension decreases from 512 to 249 gf, confirming that the control does not become delayed or divergent, even in the Moving MCDPR experiment.

In Figs. 11, 12, and 13, the calculated and measured evaluation factor values for each system that were reviewed are shown in Table 1.

It is noteworthy that despite the different average tensions maintained during cable control in stationary and moving states (∼ 60%, ∼ 37%), the maximum tensions under the conditions of using and not using the controller are similar (∼ 10%, ∼ 16%). In the case of not using HTLCA, it was observed that the tilting force caused by pure cable tension exceeded the moment equilibrium of the mechanism, leading to the mechanism tilting. On the other hand, in the case of using HTLCA, the similarity in maximum tension can be attributed to the hysteresis occurring when winding and unwinding the cable during cable control.

The improvement achieved by applying the HTLCA algorithm, expressed as a ratio, can be seen in Table 2 based on the measured and calculated results recorded in Table 1. According to the analysis of the experimental results based on Table 2, it was possible to evaluate the compensation performance for time delay and initial setup

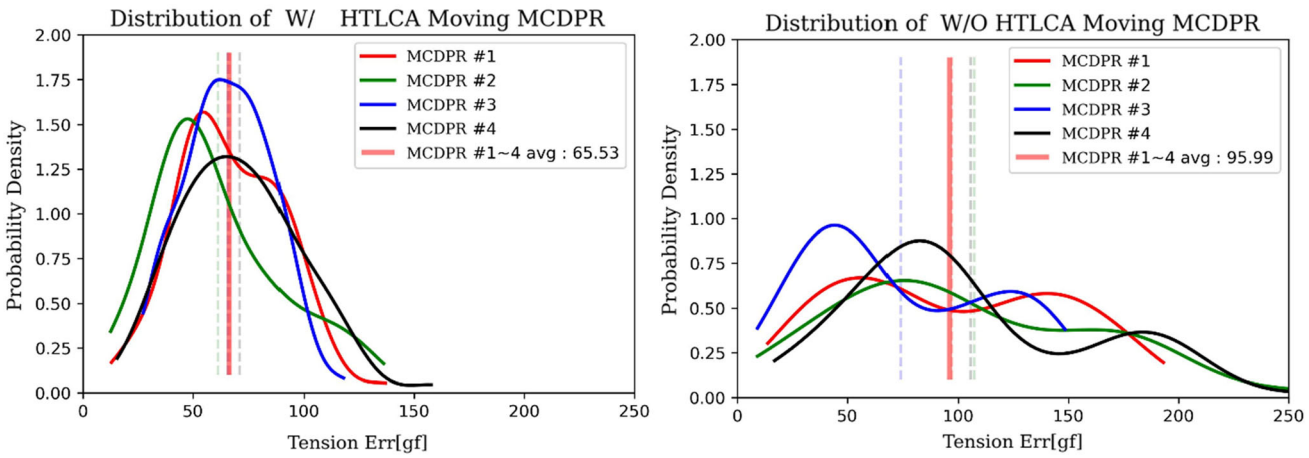

Fig. 13 Moving MCDPR KDE PDF function W/, W/O HTLCA

Table 1 Summary of MCDPR exp. data

Data	Stationary MCDPR control		Moving MCDPR control	
	W/HTLCA	W/O HTLCA	W/HTLCA	W/O HTLCA
KDE prop max	4.34	1.13	1.75	0.98
Tension load max [gf]	275	613	249	512
Avg. tension [gf]	26.35	151.98	65.53	95.99

Table 2 Comparison of HTLCA algorithm's performance at stationary, moving MCDPR exp

Data	Stationary MCDPR control	Moving MCDPR control
Reduce of tension (max load) [RE %]	− 55.13	− 51.37
Reduce of tension (KDE mean) [RE %]	− 82.66	− 31.73
KDE prop. max increased [RE %]	284.07	78.37

errors occurring in the control between MCDPR nodes in each Stationary MCDPR control experiment.

Furthermore, by conducting driving tests during MCDPR operation, the compensation performance for real-time delay, jittering, IMU integration errors, and localization errors caused by elements of MCDPR mobile robots could be evaluated comprehensively in terms of cx control delay. Overall, the results showed that the stability during control was improved with a maximum tension reduction of 55.1% and 51.37% due to the application of HTLCA. The control precision of the controller was also increased to better track the target values with an average tension reduction of 55.13% and 82.66%, which was confirmed by a 284% increase in the probability density function value. Therefore, the effectiveness of the HTLCA algorithm can be demonstrated.

4 Conclusion

The Stationary MCDPR experiment demonstrates the validity of the CDPR application by conducting end-effector motion experiments at a stationary position. Through the Stationary MCDPR experiment, the compensatory performance evaluation for time delays occurring in the control and time-invariant initial setup error of each MCDPR was confirmed. The results clearly show that the precision and stability of the control have significantly improved with the application of the HTLCA algorithm.

Next, by conducting motion tests during MCDPR operation, the compensation performance of positioning error and control delay between each MCDPR can be comprehensively evaluated. The results demonstrate a significant improvement in control precision, thus validating the effectiveness of the HTLCA algorithm.

This study designed and verified a system that can handle communication delays and localization errors, which are difficult to consider when using existing system models for MCDPR systems. The system was implemented at a low cost and in real-time. Through the application of the HTLCA algorithm and analysis of empirical data, it was confirmed that the HTLCA algorithm can maintain normal control of the end-effector even after a dynamic motion that cannot be achieved through length control due to errors caused by mobile robot movement. The HTLCA algorithm was proven to be stable and robust.

In near future, we plan to conduct a study on the effects of temperature environment on cable tension and explore methods for compensating for any changes that may occur. Additionally, we will also investigate other factors that may affect cable tension over time, such as environmental conditions and mechanical stress, to further enhance our understanding of cable behavior. By addressing these issues, we aim to develop more robust and dependable cable systems for future use.

Acknowledgements This research was carried out with the support of the RCMS project of the Korea Evaluation Institute of Industrial Technology (RCMS), "Development of InLine System for TTV Improvement and Handling of Semiconductor Ultra-Thin Wafer" (20017476) and supported by the National Research Foundation of Korea(NRF) grant funded by the Korea government(MSIT) (2021R1A2C2013053).

Author contributions Dong-Yeop Shin (DYS) developed the control algorithm, conducted experiments, performed data analysis, and wrote the main manuscript text. Byeong-Geon Kim (BGK) assisted in reviewing the control algorithm, provided advice, and contributed to the development, maintenance, and review of the experimental setup. Seok-Kyu Hong (SKH) and Jin-Hwan Lim (JHL) assisted in the development of the experimental setup and provided support during the experiments and data processing. Professor Kyoung-Su Park (KSP) supervised and guided the research as the principal investigator.

Data availability The data supporting the findings of this study, which include MCDPR robot's driving data, are available upon request. Please contact Kyoung-Su Park at pks6348@gachon.ac.kr for access to the data. Restrictions may apply to the availability of these data, which were used under license for this study.

Declarations

Conflict of interest Author Dong-Yeop Shin declares that he has no conflict of interest. Author Byeong-Geon Kim declares that he has no conflict of interest. Author Jin-huwan Lim declares that he has no conflict of interest. Author Seok-Gyu Hong declares that he has no conflict of interest. Author Kyoung-Su Park declares that he has no conflict of interest.

References

Babaghasabha R, Khosravi MA, Taghirad HD (2015) Adaptive robust control of fully-constrained cable driven parallel robots. Mechatronics 25:27–36

Bostelman RV, Albus JS (1993) Stability of an underwater work platform suspended from an unstable reference. In: Proceedings of OCEANS'93, pp 325

Bostelman RV, Dagalakis NG, Albus JS (1993) A robotic crane system utilizing the Stewart platform configuration. In: Proceedings of the ISRAM'92 conference, Santa Fe, NM

Bostelman RV, Albus JS, Murphy K, Tsai TM, Amatucci E (1994) A stewart platform lunar rover. In: Engineering construction and operations in space IV proceeding, Albuquerque, NM, Feb

Brown G (1985) Skycam: an aerial robotic camera system. In: BYTE, 122

Carpio-Alemán MA, Saltaren-Pasmino RJ, Rodríguez A, Portilla GA, Cely JS, Gonzalez-Alvarez NX, Castillo-Guerrero JM (2018) Collision and tension analysis of cable-driven parallel robot for positioning and orientation. In: 2018 IEEE international autumn meeting on power, electronics and computing (ROPEC), pp 1–6

Côté AF, Cardou P, Gosselin C (2016) A tension distribution algorithm for cable-driven parallel robots operating beyond their wrench-feasible workspace. In: 2016 16th international conference on control, automation and systems (ICCAS), pp 68–73

Fabritius M, Rubio-Gómez G, Martin C, Santos JC, Kraus W, Pott A (2023) A nullspace-based force correction method to improve the dynamic performance of cable-driven parallel robots. Mech Mach Theory 181:105177

Fabritius M, Martin C, Gomez GR, Kraus W, Pott A (2021) A practical force correction method for over-constrained cable-driven parallel robots. In: International conference on cable-driven parallel robots, pp 117–128

Gagliardini L, Gouttefarde M, Caro S (2018) Design of reconfigurable cable-driven parallel robots. In: Mechatronics for cultural heritage and civil engineering, pp 85–113

Gosselin C (2014) Cabledriven parallel mechanisms: state of the art and perspectives. Mech Eng Rev 1(1):4

Gouttefarde M, Lamaury J, Reichert C, Bruckmann T (2015) A versatile tension distribution algorithm for n-DOF parallel robots driven by n+2 cables. IEEE Trans Rob 31(6):1444–1457

Jeong JW, Kim SH, Kwak YK (1998) Design and kinematic analysis of the wire parallel mechanism for a robot pose measurement. In: Proceedings. 1998 IEEE international conference on robotics and automation (Cat. No. 98CH36146) 4:2941–2946)

Ji H, Shang W, Cong S (2020) Adaptive synchronization control of cable-driven parallel robots with uncertain kinematics and dynamics. IEEE Trans Ind Electron 68(9):8444–8454

Kawamura S, Kino H, Won C (2000) High-speed manipulation by using parallel wire-driven robots. Robotica 18(1):13–21

Korayem MH, Yousefzadeh M, Manteghi S (2017) Dynamics and input–output feedback linearization control of a wheeled mobile cable-driven parallel robot. Multibody SysDyn 40:55–73

Kraus W (2016) Force control of cable-driven parallel robots. p 24

Lafourcade P, Llibre M, Reboulet C (2002) Design of a parallel wire-driven manipulator for wind tunnels. In: Proceedings of the workshop on fundamental issues and future research directions for parallel mechanisms and manipulators, pp 187–194. Quebec City, Canada

Le Nguyen V, Caverly RJ (2021) Cable-driven parallel robot pose estimation using extended Kalman filtering with inertial payload measurements. IEEE Robot Autom Lett 6(2):3615–3622

Mao Y, Jin X, Dutta GG, Scholz JP, Agrawal SK (2014) Human movement training with a cable driven arm exoskeleton (CAREX). IEEE Trans Neural Syst Rehabil Eng 23(1):84–92

Mattioni V, Idà E, Carricato M (2022) Force-distribution sensitivity to cable-tension errors in overconstrained cable-driven parallel robots. Mech Mach Theory 175:104940

Morizono T, Kurahashi K, Kawamura S (1998) Analysis and control of a force display system driven by parallel wire mechanism. Robotica 16(5):551–563

Oh SR, Ryu JC, Agrawal SK (2006) Dynamics and control of a helicopter carrying a payload using a cable-suspended robot. J Mech Des Sep 128:1113

Pedemonte N, Rasheed T, Marquez-Gamez D, Long P, Hocquard É, Babin F, Caro S (2020) Fastkit: a mobile cable-driven parallel robot for logistics. Advances in robotics research: from lab to market: ECHORD++: robotic science supporting innovation. Springer, Cham, pp 141–163

Rasheed T, Long P, Marquez-Gamez D, Caro S (2018) Tension distribution algorithm for planar mobile cable-driven parallel robots. In: Cable-driven parallel robots: proceedings of the third international conference on cable-driven parallel robots, pp 268–279

Rasheed T, Long P, Roos AS, Caro S (2019) Optimization based trajectory planning of mobile cable-driven parallel robots. In: 2019 IEEE/RSJ International Conference on Intelligent Robots and Systems (IROS), pp 6788–6793. IEEE

Rosati G, Gallina P, Masiero S Rossi A (2005) Design of a new 5 d.o.f. wire-based robot for rehabilitation. In: 9th International conference on rehabilitation robotics, 2005. ICORR 2005., pp. 430–433

Tan H, Nurahmi L, Pramujati B, Caro S (2020) On the reconfiguration of cable-driven parallel robots with multiple mobile cranes. In: 2020 5th International conference on robotics and automation engineering (ICRAE), pp 126–130

Tho TP, Thinh NT (2022) An overview of cable-driven parallel robots: workspace, tension distribution, and cable sagging. Math Probl Eng 2022:2199748

Wang W, Tang X, Shao Z, Yang J, Yi W (2014) Design and analysis of a wire-driven parallel mechanism for low-gravity environment simulation. Adv Mech Eng 6:810606

Xu J, Park KS (2020) A real-time path planning algorithm for cable-driven parallel robots in dynamic environment based on artificial potential guided RRT. Microsyst Technol 26:3533–3546

Xu J, Park KS (2022) Kinematic performance-based path planning for cable-driven parallel robots using modified adaptive RRT. Microsyst Technol 28(10):2325–2336

Xu J, Kim BG, Feng X, Park KS (2023a) Online motion planning of mobile cable-driven parallel robots for autonomous navigation in uncertain environments. Complex Intell Syst 10:397–412

Xu J, Kim BG, Park KS (2023b) A collaborative path planning method for mobile cable-driven parallel robots in a constrained environment with considering kinematic stability. Complex Intell Syst 9(5):4857–4868

Yao R, Li H, Zhang X (2013) A modeling method of the cable driven parallel manipulator for FAST. Cable-driven parallel robots. Springer, Berlin, pp 423–436

Zhang Z, Shao Z, Wang L, Shih AJ (2018) Optimal design of a high-speed pick-and-place cable-driven parallel robot. In: Cable-

driven parallel robots: proceedings of the third international conference on cable-driven parallel robots, pp 340–352